A methodology for detecting interfacial debonding in clay/epoxy nanocomposites

JAE-HYUN KIM, GALE A. HOLMES * and CHAD R. SNYDER

National Institute of Standards and Technology, Polymers Division, Characterization and Methods Development Group, 100 Bureau Drive Stop 8541, Gaithersburg, MD 20899-8541, USA

Abstract—A novel methodology is presented for detecting the onset of debonding in clay-based nanocomposites. The procedure is based on constant illumination of the test specimen as it is subjected to tensile deformation by sequential strain-steps. After each strain-step, an image of the specimen is taken along its gauge length using a digital camera and the image is stored in a computer for later analysis using image analysis software. Test results from a nanocomposite containing a weak interface between the clay and the matrix indicate that interface debonding begins to occur above 1% strain, as evidenced by a reduction in the transmitted light through the specimen with increasing strain. Based on related research, the darkening of the specimen was interpreted as clay/matrix debonding. In contrast to the approximately 11% failure strain of the base epoxy resin, the nanocomposite specimen with the weak interface failed at 3.6% strain.

1. INTRODUCTION

The potential application of clay-based nanocomposites in structural applications has led to a broadening of the research focus on these materials to include discussions about their strain-to-failure relative to the unmodified polymer. Early researchers envisioned using nanotechnology to achieve significant increases in base material performance without significant sacrifices to key engineering properties that are critical to their success in such applications. As an example, the tensile strength, tensile modulus and strain-to-failure of clay nanocomposites prepared from polyurethane [1, 2] and elastomeric epoxy [3] resins have been shown to increase relative to neat matrices. Interestingly, since the clay is treated with an alkyl ammonium salt to facilitate exfoliation, these property improvements are achieved

---

*To whom correspondence should be addressed. Tel.: (1-301) 975-5280. Fax: (1-301) 975-3928.
E-mail: gale.holmes@nist.gov

without the "formal" establishment of significant adhesion forces between the nanomaterial and the matrix. For conventional composites, poor adhesion between the reinforcement and the matrix generally results in a reduction in engineering performance properties [4].

However, similar results on nanocomposites made from glassy epoxies [5–7], which are often used in structural composites, indicate that, like fibrous composites, modulus and strength increases are achieved at the expense of the base material's strain-to-failure. Because conventional composites modified with clay and other nanomaterials, e.g., carbon nanotubes, have the potential of increasing a composite's compressive strength, reducing its flammability and increasing its electrical conductivity, this change in performance of glassy epoxy resins relative to elastomeric epoxy resins is important and requires further study. In addition, research on TPO (thermoplastic olefin) nanocomposites targeted for semi-structural automotive applications exhibit a similar reduction in the strain-to-failure with nanoclay inclusion [8]. These materials have 10% or higher mass fractions of clay, relative to current commercial TPOs that have 3% or lower mass fractions of clay.

These results and results from other researchers suggest a complicated set of factors influencing the interaction between the nanomaterial and the matrix. Among these are the adhesion strength of the nanomaterial/matrix interface; the intrinsic toughness of the host matrix; the dispersion of the nanomaterial within the matrix; and the size, shape, and exchange capacity of the nanomaterial.

To better understand the importance and dynamics of these interactions, test methodologies that detect and quantify the onset of failure and the nucleation of critical flaws in nanocomposite materials are needed. In this paper, the responses of clay nanocomposites that contain strong and weak interfaces are monitored as the test specimens are subjected to tensile loads using optical imaging technology. To achieve variations in clay/matrix interfacial strength the clay was treated with an often-used non-bonding amine additive and an amine additive that has the potential of bonding to the epoxy matrix. The manner in which optical imaging is used to detect the onset of clay matrix debonding is discussed.

2. EXPERIMENTAL

2.1. Materials

Sodium montmorillonite (Na^+ Cloisite) and montmorillonite treated with dimethyl, benzyl, hydrogenated tallow quaternary ammonium chloride (Cloisite 10A) were obtained from Southern Clay Products (Gonzales, TX, USA). The diglycidyl ether of 1,4-butanediol (CAS No. 2425-79-8; trade name: Araldite RD-2; common name: DGEBD) and 1,3-phenylenediamine (CAS No. 108-45-2) were obtained from Sigma-Aldrich (St. Louis, MO, USA). For 12-aminolauric acid (CAS No. 693-57-2), TCI America (Portland, OR, USA) was utilized as a resource. Many suppliers produce the diglycidyl ether of bisphenol-A (CAS No. 25068-38-6; common name:

DGEBA); however, the product obtained through Miller-Stephenson had the trade name Shell Epon Resin 828. All products were used as received without further purification.

2.2. Preparation of C_{12}-montmorillonite

Sodium montmorillonite was treated with 12-aminolauric acid using the procedure outlined by Usuki *et al.* [9] where solutions A and B are mixed to effect the exchange reaction. Solution A was prepared by placing 24 mmol of the ω-amino acid into a 1000-ml beaker containing 200 ml of water that had been preheated to 80°C. To this mixture 2.4 ml of concentrated hydrochloric acid (HCl) was added. Solution B was prepared by adding 10 g of montmorillonite to 1000 ml of 80°C water contained in a 1500 ml beaker and stirring. Solution A was then added to Solution B and stirred vigorously for 10 min.

The treated montmorillonite clay was then filtered and washed 4 times with 1000 ml aliquots of 80°C water. The filtrate was then freeze-dried overnight with a Virtis Automatic Freeze Dryer (Model No. 10-010) using a dry ice/ethanol bath for freezing the filtrate. The freeze-dried material was then vacuum dried at 100°C overnight in a Fisher Scientific IsoTemp Vacuum Oven (Model 281A) using a dry ice/ethanol bath to trap the volatiles. The treated clay material was then cooled down under vacuum to room temperature and slowly vented with room air. The product was then crushed with a mortar and pestle and stored in a plastic bottle until use. In this paper, this material was named C_{12}-montmorillonite. In contrast to Cloisite 10A, this material has the capability of increasing the adhesion between the clay and the host matrix through the reaction of the acid group with the epoxide groups in the DGEBA monomer.

2.3. Preparation of dogbone tensile test (DBTT) specimen

The molds for preparing the dogbone tensile test (DBTT) specimens were made with silicone rubber (General Electric) following the procedure described by Herrera-Franco and Drzal [10]. All molds were post-cured at 150°C and rinsed with acetone prior to use. Using Cloisite 10A and C_{12}-montmorillonite, DBTT specimens containing approximately 2.5% mass fraction of treated clay were prepared by adding approximately 0.154 g of clay to 6 g of epoxy mixture. The epoxy mixture consisted of 80% mass fraction of DGEBA and 20% mass fraction of DGEBD. The 10-ml beakers containing the clay/epoxy mixtures and a non-clay/epoxy mixture (blank) were then covered with Dura Seal stretch film and then heated to 50°C, overnight, on a Corning Stirrer Hot Plate (Model PC-620) while stirring the mixture with small magnetic stirrers.

The beakers containing the epoxy/clay mixtures were then placed in a vacuum oven (Fisher Scientific IsoTemp Vacuum Oven, model 281A) set at 50°C. Stoichiometric amounts of *meta*-phenylenediamine (*m*-PDA) crystals (approximately 0.8 g) were placed into another vacuum oven set at 65°C. After the *m*-PDA crystals were

completely melted, the silicone rubber molds were placed into a third vacuum oven that was preheated to 75 °C at 20 kPa vacuum, for 20 min. This last procedure dries the mold and minimizes the formation of air bubbles during the curing process.

Approximately 9 min before the preheated molds were removed from the oven, the *m*-PDA was poured into each clay/epoxy mixture or epoxy only mixture and thoroughly mixed. The resulting mixture was then placed into the vacuum oven and degassed for approximately 7 min. After 20 min, the preheated molds were removed from the oven and filled with the resin mixture using 10-ml disposable syringes. The filled molds were then placed into a programmable oven (Blue M, model MP-256-1). A cure cycle of 3 h at 60 °C followed by 2 h of post-curing at 121 °C was used.

2.4. Automated tensile testing apparatus

Tests were carried out on the automated tensile testing machine shown in Fig. 1. The instrument is equipped with a Fostec (150 W) illumination system and a digital camera that scans the gauge length of the dogbone specimen after each strain increment. Before testing, samples were polished with emery papers No. 800 and 2400 to remove stress concentration sites at the edges of the sample. To facilitate strain measurements, transverse fiducial marks (approximately 10 mm apart) were applied to each end of the specimen gauge length by a blue color permanent pen. Strains at each step were calculated using the scanned images at each step. In the absence of premature specimen failure, the total strain in the sample at the end of the test was programmed to be about 8.0%.

Specimen slippage during testing was minimized by placing the specimen in the grips with moderate tightness. The specimen was then loaded in tension by the sequential application of strain-steps. During the test, 35 strain-steps were applied and the total deformation was approximately 3.0 mm. Each strain-step was applied at a rate of 85 μm/s and the average deformation in the specimen during each strain-step was 85.7 μm. The delay time between the applications of successive strain-steps was 10 min. The image was scanned after every strain-step using a movable camera. The digital image was saved automatically in the computer. The gauge length scanned was 23 mm. In the absence of premature failure of the test specimens, the sample was unstressed and removed after 35 strain-steps.

2.5. Image analysis

In each image the data between the fiducial marks were analyzed using the histogram image analysis function in Corel Photo-Paint 8. The histogram feature is a read-only horizontal bar chart that plots the brightness value of every image pixel. In this analysis program, pixel values range from 0 (black) to 255 (white), and the histogram indicates how many pixels are at a given brightness level. The histogram from each image conformed to a bell curve and therefore, the statistical outputs (e.g., mean and standard deviation) were used to compare the change in image between
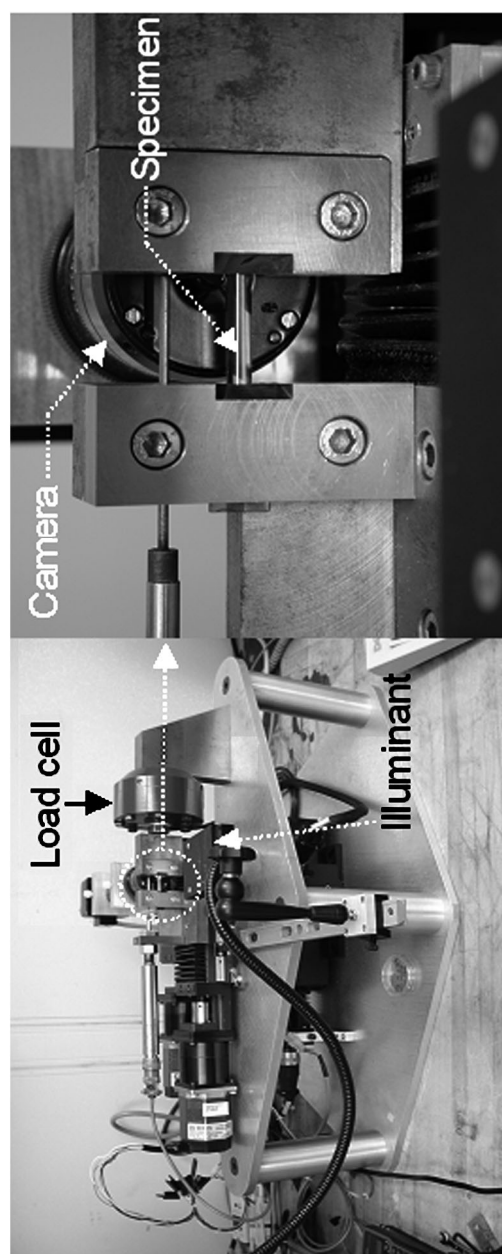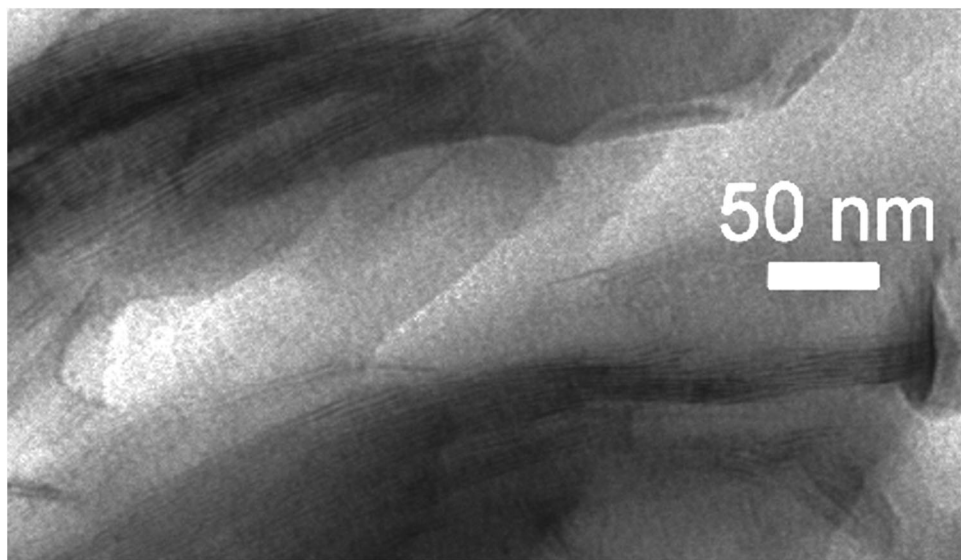
Figure 1. Automated tensile testing machine.

Figure 2. Transmission electron microscopy (TEM) image of C_{12}-montmorillonite/epoxy nanocomposite.

strain-steps. Uncertainties in this analysis approach were determined in accordance with propagation of error techniques [11].

3. RESULTS AND DISCUSSION

3.1. Deposition of clay mixtures

The epoxy-clay mixtures of Cloisite 10A and C_{12}-montmorillonite were transparent and cloudy, respectively, prior to the addition of the *m*-PDA curing agent. Addition of the *m*-PDA curing agent did not immediately cause the Cloisite 10A epoxy mixture to turn cloudy or the C_{12}-montmorillonite epoxy mixture to turn clear. However, at the end of the curing cycle, both nanocomposites were somewhat cloudy. The cloudiness is supported by the transmission electron microscopy (TEM) image (Fig. 2) showing an intercalated morphology for the C_{12}-montmorillonite/epoxy nanocomposite. However, with the 2.5% mass fraction clay loading, the 2-mm-thick dogbone specimens were transparent enough to clearly read the text on a printed paper placed beneath the specimen.

3.2. Stress–strain response

The small–strain moduli of the diglycidyl ether of bisphenol-A (DGEBA)/diglycidyl ether of butanediol (DGEBD)/*m*-PDA epoxy and the nanocomposites prepared from this resin with Cloisite 10A and C_{12}-montmorillonite were found to be similar, with values of 2.83 ± 0.19 GPa, 3.08 ± 0.15 GPa and 2.55 ± 0.04 GPa, respectively,

○ Epoxy (DGEBA/DGEBD/m-PDA)
● Epoxy with 2.51% mass fraction of Closite-10A
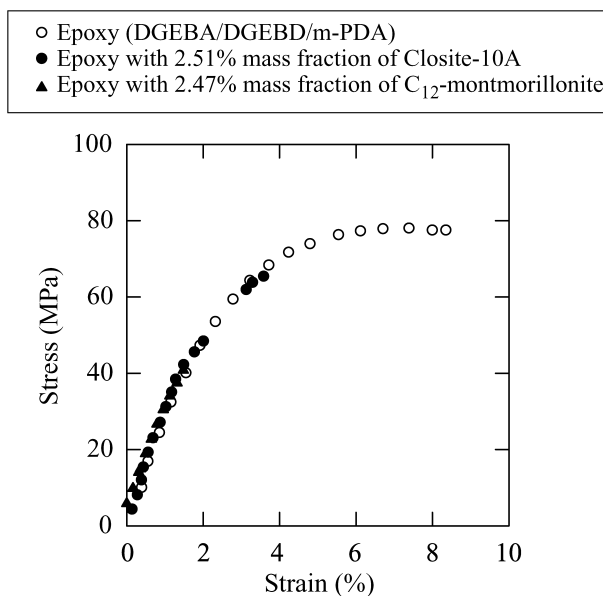▲ Epoxy with 2.47% mass fraction of C_{12}-montmorillonite

Figure 3. Stress–strain curves of DGEBA/DGEBD/*m*-PDA epoxy resin and this resin loaded with approximately 2.5% mass fraction of Cloisite 10A and C_{12}-montmorillonite.

where the ± values represent one standard deviation about the average value and are taken as an estimate of the standard uncertainty (Fig. 3). This is not surprising since the dramatic increase in modulus usually observed with nanoclay inclusion typically occurs at much higher clay loadings (approximately 15%).

The strain-to-failure of the Cloisite 10A and C_{12}-montmorillonite nanocomposites were found to be 3.6% and 1.5%, respectively. The DGEBA/DGEBD/*m*-PDA epoxy strain-to-failure without clay has been shown in previous experiments to be approximately 10–11%. In Fig. 3, the DGEBA/DGEBD/*m*-PDA epoxy was taken to 8.4% strain without specimen failure. The reduction in the strain-to-failure with nanoclay inclusion is consistent with previous research results involving glassy epoxy resins.

3.3. Nanoclay-epoxy composite failure behavior

Under constant illumination, images of a DGEBA/DGEBD/*m*-PDA epoxy resin dogbone specimen were taken as the specimen was deformed by the sequential application of strain-steps (see Fig. 4). From these images it is clear that the intensity of the transmitted light through the specimen does not change with increasing strain. The strain in the gauge section was quantified by measuring the distance between the fiducial marks that were made on the specimen.

In Fig. 5, the image changes of a Cloisite 10A epoxy-nanocomposite and a C_{12}-montmorillonite/epoxy nanocomposite are shown in a side-by-side comparison. Each image is truncated to show only the data between the fiducial marks. The
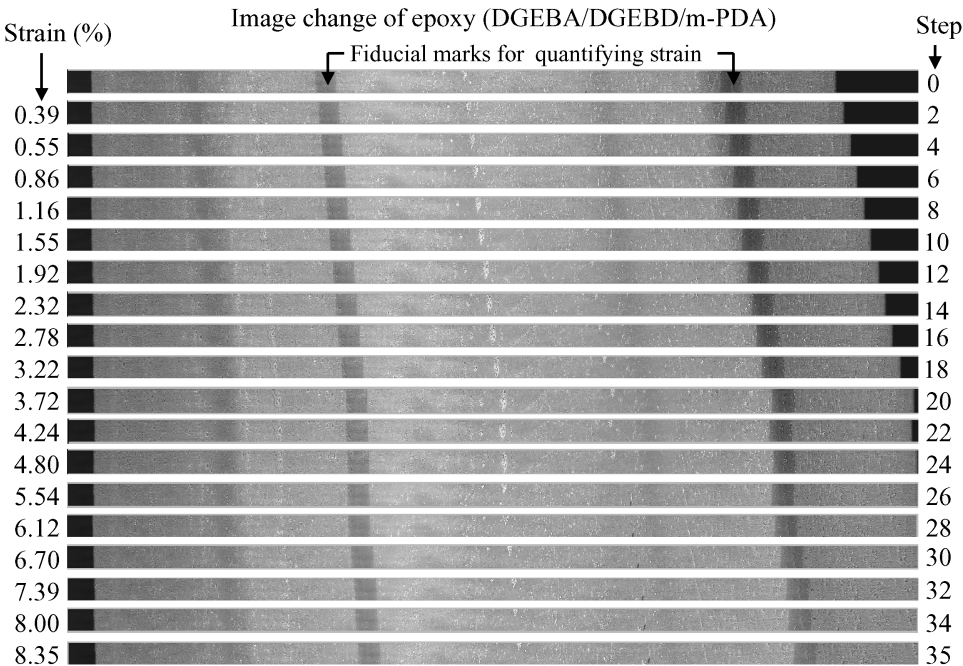
Strain (%) Image change of epoxy (DGEBA/DGEBD/m-PDA) Step

┌ Fiducial marks for quantifying strain ┐

Strain (%)	Step
	0
0.39	2
0.55	4
0.86	6
1.16	8
1.55	10
1.92	12
2.32	14
2.78	16
3.22	18
3.72	20
4.24	22
4.80	24
5.54	26
6.12	28
6.70	30
7.39	32
8.00	34
8.35	35

Figure 4. Change in image of DGEBA/DGEBD/*m*-PDA dogbone specimen with increasing strain.

images of the Cloisite 10A nanocomposite above 1% strain darken with increasing deformation. The darkening of the specimens is clearly evident at 1.3–1.5% strain (strain steps 10 and 11) and the fiducial marks (not shown) used to calculate the strain in the specimen were barely visible at strains above 2% (strain step 14). On strain step 18 the illumination from the light source was increased making the fiducial marks (not shown) visible again.

Based on the reduction of transmitted light that occurs in the debonded region surrounding a fiber break in conventional glass fiber composites (Ref. [12] and references therein), the image change with increasing strain has been interpreted in terms of clay-matrix interface debonding. Since Cloisite 10A, like most of the current clay surface treatment technology, contains a hydrophobic alkyl ammonium salt, covalent bonding between the treated clay and the host matrix is formally precluded. Therefore, the interface between the clay and the matrix is weak and should be prone to debonding under tensile loads.

To further explore this line of reasoning, adhesion at the clay/matrix interface was promoted by treating Na^+ montmorillonite with readily available 12-aminolauric acid to prepare the C_{12}-montmorillonite clay initially used by Usuki *et al.* [9] in the preparation of clay/nylon nanocomposites. Although the carboxylic acid functional group is not the ideal functional group for competing with the amine-epoxy curing reaction, research results from the toughening of epoxy resin with carboxyl-terminated polybutadiene acrylonitrile (CTBN) rubber indicate that covalent bonding between the clay and the host matrix may be facilitated by first placing the
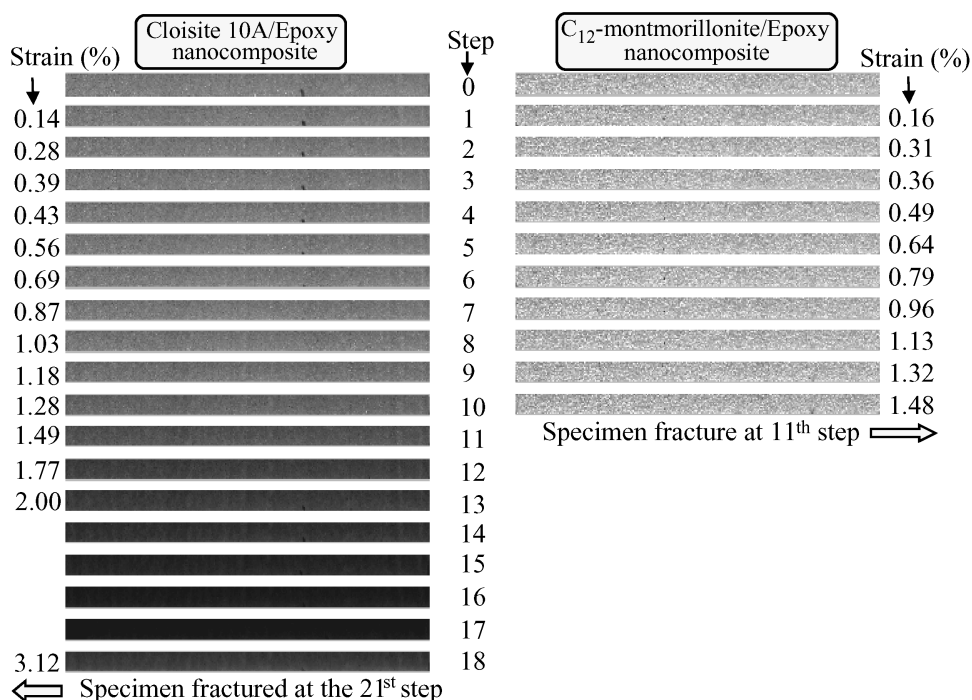
Figure 5. Changes in images of Cloisite 10A and C_{12}-montmorillonite/epoxy nanocomposites with increasing strain.

C_{12}-montmorillonite clay into the epoxy resin for a time to promote reaction between the epoxide and the carboxylic acid groups. After this procedure, the amine curing agent is then added to complete the cure of the epoxy resin.

As shown in Fig. 5, no change in image intensity of the C_{12}-montmorillonite epoxy nanocomposite occurred prior to specimen failure, approximately 1.6% strain. As previously discussed, a reduction in the transmitted light in the Cloisite 10A nanocomposite was visually observable at 1.3–1.5% strain. Since the failure strain of this specimen is at the point where darkening of the Cloisite 10A becomes evident, these results suggest that the darkening of the Cloisite 10A specimen is due only to clay-matrix debonding at the weak interface. Therefore, a parallel investigation was initiated where covalent bonding between the clay and the epoxy matrix was achieved by depositing a 1:3 to 2:3 molar mixture of bonding and non-bonding alkyl amines onto the clay surface. These epoxy nanocomposites failed at a higher strain level (2.4–2.6%) and no change in the image intensity of the specimen was observed prior to failure. The specifics of this investigation will be reported elsewhere. These results further support the assumption of the authors that the darkening of the Cloisite 10A nanocomposite with increasing strain is due to debonding at the weak clay-matrix interface.

The relative change in the transmitted light through a test specimen was quantified by using the histogram feature of the imaging software. In Fig. 6, the relative im-
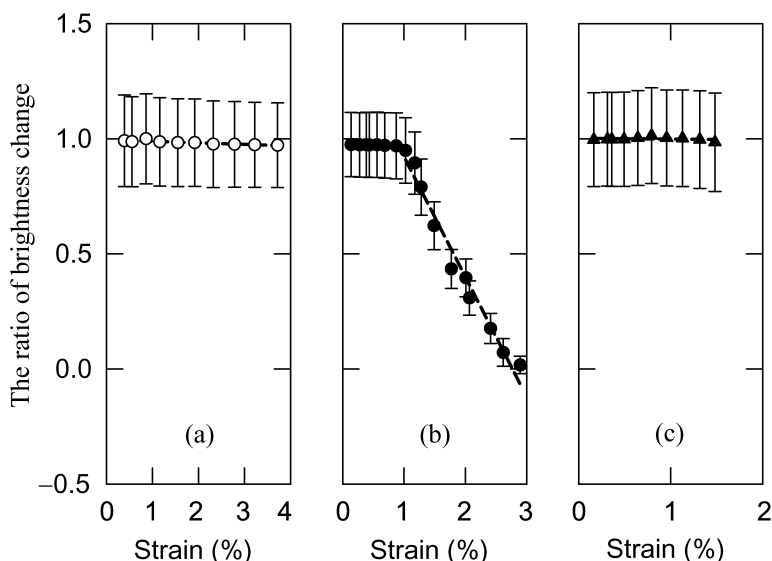
Figure 6. The ratio of brightness change in DGEBA/DGEBD/*m*-PDA with (a) no clay, (b) 2.51% Cloisite 10A and (c) 2.47% C_{12}-montmorillonite. All calculations compared to the unstrained state.

age change below 3% strain is shown for the DGEBA/DGEBD/*m*-PDA epoxy resin dogbone specimen (Fig. 6a), the Cloisite 10A-epoxy nanocomposite (Fig. 6b), and the C_{12}-montmorillonite/epoxy nanocomposite. The results depicted in Fig. 6 confirm what is visually observed in Figs 4 and 5. While the DGEBA/DGEBD/*m*-PDA epoxy resin dogbone specimen and the C_{12}-montmorillonite/epoxy nanocomposite show no change in intensity with increasing strain, an abrupt change in the transmitted light above 1.0% strain occurs in the Cloisite 10A-epoxy nanocomposite. The error bars represent the standard uncertainty in the image intensity change relative to the intensity observed at zero deformation.

The stress applied to the Cloisite 10A test specimen at the onset of debonding was approximately 35 MPa and the applied stress prior to failure was 65 MPa. The testing of a second sample yielded similar results. The debond initiation stress observed in this nanocomposite is similar to the debond initiation stress observed in cruciform test specimens composed of silicon carbide fibers embedded in a room-temperature-cured DGEBA-Jeffamine D230 matrix, 33–41 MPa [13, 14].

4. CONCLUSIONS

The results indicate that clay-matrix debonding occurs in nanocomposite specimens containing weak interfaces and that the onset of this process can be observed by a tensile deformation procedure that incorporates constant illumination of the test specimen. In the Cloisite 10A nanocomposite, the debonding process begins at approximately 1% strain and continues until the specimen fails at 3.6% strain. The

process that nucleates the critical flaws (i.e., growing interface crack, nucleation of sub-critical cracks, or other mechanism) will be the subject of future research.

Although the creation of covalent bonds at the clay-matrix interface was achieved by the treatment of Na^+ montmorillonite with 12-aminolauric acid, the strain-to-failure of the resulting nanocomposite was less than the nanocomposite with the weak interface, and the strains-to-failure of both nanocomposites were less than the base epoxy resin. Because the nanocomposites were not completely exfoliated, the failure strains observed in this report may be less than those that may be observed when exfoliated nanoclay particles are incorporated in glassy epoxies. The results, however, do suggest the need for continued research. Also, the results presented here provide a framework for quantifying the failure behavior of nanocomposites.

Acknowledgements

REFERENCES

1. Z. Wang and T. J. Pinnavaia, *Chem. Mater.* **10**, 3769 (1998).
2. C. Zilg, R. Thomann, R. Mulhaupt and J. Finter, *Adv. Mater.* **11**, 49 (1999).
3. T. Lan and T. J. Pinnavaia, *Chem. Mater.* **6**, 2216 (1994).
4. G. A. Holmes, to be Submitted to Material Science & Engineering R-Reports.
5. T. Lan, P. D. Kaviratna and T. J. Pinnavaia, *Chem. Mater.* **7**, 2144 (1995).
6. X. Kornmann, R. Thomann, R. Mulhaupt, J. Finter and L. Berglund, *J. Appl. Polym. Sci.* **86**, 2643 (2002).
7. X. Kornmann, R. Thomann, R. Mulhaupt, J. Finter and L. Berglund, *Polym. Eng. Sci.* **42**, 1815 (2002).
8. S. Wu and C.-J. Chou, in: *Proc. Tenth Annual International Conference on Composites/Nano Engineering*, New Orleans, LA, p. 773 (2003).
9. A. Usuki, M. Kawasumi, Y. Kojima, A. Okada, T. Kurauchi and O. Kamigaito, *J. Mater. Res.* **8**, 1174 (1993).
10. P. J. Herrera-Franco and L. T. Drzal, *Composites* **23**, 2 (1992).
11. H. H. Ku, *J. Res. NBS — C. Eng. Inst.* **70C**, 263 (1966).
12. G. A. Holmes, R. C. Peterson, D. L. Hunston and W. G. McDonough, *Polym. Composites*, in press (2006).
13. G. Tandon, R. Kim and V. Bechel, *J. Composite Mater.* **36**, 2667 (2002).
14. V. Bechel and G. Tandon, *Exp. Mech.* **42**, 200 (2002).